

Report 82-9F3-SIMFN-R1
Contract No. N00014-81-C-0632

10

AD-A132 980

INVESTIGATION OF ION ENERGY DEPOSITION IN SOLIDS

W. J. Choyke, J. A. Spitznagel, and R. M. More
Westinghouse Research and Development
1310 Beulah Road
Pittsburgh, PA 15235

July 16, 1982

Final Report for Period July 7, 1981 - June 30, 1982

Approved for Public Distribution

Distribution Unlimited

Prepared for

United States Navy
Office of Naval Research
Ballston Center
800 North Quincy Street
Arlington, VA 22217

DTIC FILE COPY

83 09 26 087

S

SEP 27 1983

A

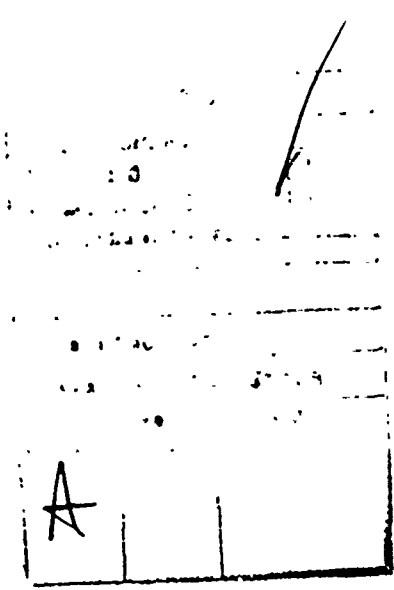
REPORT DOCUMENTATION PAGE		READ INSTRUCTIONS BEFORE COMPLETING FORM
1. REPORT NUMBER	2. GOVT ACCESSION NO.	3. RECIPIENT'S CATALOG NUMBER
	AD A132980	
4. TITLE (and Subtitle)	5. TYPE OF REPORT & PERIOD COVERED	
INVESTIGATION OF ION ENERGY DEPOSITION IN SOLIDS	Final Report 7 July 1981 to 30 June 1982	
	6. PERFORMING ORG. REPORT NUMBER	
	82-9F3-SIMFN-R1	
7. AUTHOR(s)	8. CONTRACT OR GRANT NUMBER(s)	
W. J. Choyke J. A. Spitznagel R. M. Moore(Consultant, Lawrence Livermore Lab)	N00014-81-C-0632	
9. PERFORMING ORGANIZATION NAME AND ADDRESS	10. PROGRAM ELEMENT, PROJECT, TASK AREA & WORK UNIT NUMBERS	
Westinghouse R&D Center 1310 Beulah Road Pittsburgh, PA 15235		
11. CONTROLLING OFFICE NAME AND ADDRESS	12. REPORT DATE	
United States Navy, Office of Naval Research Ballston Center, 800 North Quincy Street Arlington, VA 22217	July 16, 1982	
	13. NUMBER OF PAGES	
14. MONITORING AGENCY NAME & ADDRESS (if different from Controlling Office)	15. SECURITY CLASS. (of this report)	
	U	
	15a. DECLASSIFICATION DOWNGRADING SCHEDULE	
16. DISTRIBUTION STATEMENT (of this Report)		
Approved for public release - distribution unlimited.		
17. DISTRIBUTION STATEMENT (of the abstract entered in Block 20, if different from Report)		
Approved for public release - distribution unlimited.		
18. SUPPLEMENTARY NOTES		
19. KEY WORDS (Continue on reverse side if necessary and identify by block number)		
ion, damage, energy, deposition, theories, recoil, spectra, mass, defects, cascades, subcascades, bombardment, silicon, implants, elastic displacement, channeling, knock-on-atoms, collisions, final, state		
20. ABSTRACT (Continue on reverse side if necessary and identify by block number)		
A combined theoretical and experimental study of primary recoil spectra effects or radiation damage in silicon is presented. Calculations determined how the damage energy is partitioned into free defects and cascades by fast collisions. The theory also showed that on a time scale $\sim 10^{-14}$ sec, a very weak mass dependence of the lattice damage is to be expected. Channeling experiments were then performed on <111> single crystal silicon implanted with 1.0 MeV ^{20}Ne , 0.5 MeV ^4He and 75 keV ^1H . Energies and fluences of the ions were matched such that over the first 0.3 μm the damage energy deposited and the rate of energy		

20. Abstract (Continued)

deposition were the same for all species. The experimental data were analyzed assuming that equivalent primary damage states will evolve into statistically equivalent final damage states at high fluences. They confirm that the final damage is essentially independent of the mass of the bombarding ion.

CONTENTS

	<u>Page</u>
List of Figures.	v
Preface.	vii
Summary.	viii
1. Introduction	1
2. PKA Spectra and Cascades	3
3. Experimental Background.	5
3.1 Selection of Target Materials	5
3.2 Choice of Bombarding Ions and Implant Conditions. .	5
4. Experimental Procedures.	7
5. Results and Discussion	8
5.1 Subcascade Spectra.	8
5.2 Backscattering Data	11
6. Conclusions.	18
7. References	19



LIST OF FIGURES

	<u>Page</u>
Figure 1. Damage energy deposited per unit length as a function of depth near the surface of a silicon sample for 75 keV ^1H , 0.5 MeV ^4He and 1.0 MeV ^{20}Ne . The appropriate parameters for normalizing to the ^{20}Ne curve are given on the figure.	6
Figure 2. Calculations of the direct and reduced energy spectra for various PKA energies. The direct spectrum shows the energy deposited in secondary events by PKAs of specified energy. E_d is 1.6 keV and E_u is 12 keV in this figure. As the PKA energy rises, a larger fraction of the energy is delivered to energetic ($E > E_u$) secondaries (shaded box). The reduced spectrum results from distributing the energy of the shaded box into energy of free defects, cascades and electrons. In the reduced spectrum, the cascade energy is a constant multiple of the free defect energy, independent of PKA energy.	9
Figure 3. Schematic representation of defect and subcascade formation as a function of PKA energy.	10
Figure 4. Comparison of normalized yield spectra ($\langle 111 \rangle$ axis) for silicon implanted with 1.0 MeV Ne^+ to a fluence of 1.39×10^{15} ions/cm 2 and nonimplanted silicon (curve marked (n-1)). Implants were made at approximately 5° off-axis and all spectra were obtained with a 1.5 MeV ^4He beam	12
Figure 5. Comparison of normalized yield spectra ($\langle 111 \rangle$ axis) for silicon implanted with 0.5 MeV He^+ to a fluence of 5.31×10^{16} ions/cm 2 and nonimplanted silicon (curve marked (n-1)). Implants were made at approximately 5° off-axis and all spectra were obtained with a 1.5 MeV ^4He beam	13

LIST OF FIGURES (Continued)

	<u>Page</u>
Figure 6. Comparison of normalized yield spectra (<111> axis) for silicon implanted with 75 keV H ⁺ to a fluence of 1.37×10^{17} ions/cm ² and nonimplanted silicon (curve marked (n-i)). Implants were made at approximately 5° off-axis and all spectra were obtained with a 1.5 MeV ⁴ He beam.	14
Figure 7. Plot of the dechanneling rate as a function of depth into the crystal for 1 MeV ²⁰ Ne, 0.5 MeV ⁴ He and 75 keV ¹ H at the dose equivalent to 1.39×10^{15} ²⁰ Ne/cm ²	16

PREFACE

In the Fall of 1980, we had high hopes for continuing our long-term study of energy deposition due to ion bombardment in metals and semiconductors. However, due to shifts in ONR personnel and program priorities, we reformulated our research goals to study the stopping of ions under "exotic" conditions. We felt that since high-intensity pulsed irradiation is technologically close at hand, this study appeared timely and worthwhile. Nevertheless, in the decision process this direction was considered to be too far afield from the program objectives. Very kindly, ONR did grant us funding for what was to be an extension to ONR N00014-76-C-0482, in order to tidy things up and write a final report. Due to further delays, however, it became impossible to extend the old contract and a new one had to be issued. This meant that a final report now had to be written in the late Fall of 1981 covering the period 7 January 1976 to 31 October 1981.

This rather complicated series of events left the new contract N00014-81-C-0632 with its main purpose accomplished and reported upon. However, not anticipating all these events early enough, we had started a research effort on the simulation of radiation damage in semiconductors quite complementary to our previous work in metals. By scraping together various resources, we have been able to complete the studies on single crystal Si and give these results here as the main body of this final report. Readers interested in our previous work are referred to the final report of contract N00014-76-C-0482.

about 10 to the minus 14th power

SUMMARY

A combined theoretical and experimental study of primary recoil spectra effects or radiation damage in silicon is presented. Calculations determined how the damage energy is partitioned into free defects and cascades by fast collisions. The theory also showed that on a time scale $\sim 10^{-14}$ sec, a very weak mass dependence of the lattice damage is to be expected. Channeling experiments were then performed on $\langle 111 \rangle$ single crystal silicon implanted with 1.0 MeV ^{20}Ne , 0.5 MeV ^4He , and 75 keV ^1H . Energies and fluences of the ions were matched such that over the first 0.3 μm , the damage energy deposited and the rate of energy deposition were the same for all species. The experimental data were analyzed assuming that equivalent primary damage states will evolve into statistically equivalent final damage states at high fluences. They confirm that the final damage is essentially independent of the mass of the bombarding ion.

micrometers

1. INTRODUCTION

A primary concern in the simulation of neutron damage by ion beams and in the study of ion beam induced damage in general revolves around how the initiating (incident) particle interacts with the target to produce recoil atoms and atomic displacements. Some of the key questions relate to understanding how the energy is partitioned in the host, both on a fast collision time scale of 10^{-14} to 10^{-12} sec and on the longer time scale associated with cascade collapse. One needs to determine whether the amount of damage created by particles of different mass and energy depends on the total energy deposited into displacement processes. Another fundamental question pertains to the spatial distribution or degree of localization of the damage produced by recoiling atoms of different energies.

Considerable interest in the above problems prompted a combined theoretical and experimental study of primary recoil spectra effects at the HEIBS (High Energy Ion Bombardment Simulation) facility at the University of Pittsburgh.* The theoretical effort was aimed at calculating the relative energy deposited in free defects and subcascade regions for energetic recoils ($E \geq 1$ keV) before annealing.

There is considerable experimental evidence and some previous theoretical calculations which suggest that the energy in a displacement cascade does not increase indefinitely with increasing primary recoil atom energy in materials where cascades can occur. Rather, above some energy, E_u , cascades split into well-defined separate subcascade regions. Merkle⁽¹⁾_u has summarized much of the experimental evidence for subcascade

*The HEIBS effort is jointly comprised of Westinghouse R&D Center and University of Pittsburgh personnel.

formation, and their existence has also been suggested by computer simulations of atomic displacement cascades using the binary-collision approximation.^(2, 3) In this work, the subcascade production probability was calculated on the basis of the LSS-LNS theory of ion scattering and energy loss^(4, 6) and clearly shows that the primary damage state is remarkably independent of the ion species and its PKA spectrum.

Since it is almost impossible experimentally to determine the partitioning of energy into subcascades and "free" defects on the fast collision time scale, experiments were designed on the premise that statistically equivalent primary damage states (calculated) will evolve into statistically equivalent final damage states at high fluences. This means that techniques used to "measure" the resulting damage, such as Rutherford backscattering/channeling experiments, should not be able to distinguish between damage resulting from ions of different mass and energy (and therefore PKA spectra) if the total damage energy deposited into the target and the rate of energy deposition are the same for all ions. This presupposes that the ions are sufficiently energetic to launch recoils which can produce cascades. To determine whether differences in the primary recoil energy spectra result in measurably different damage states, single crystal silicon targets were bombarded with ions of different mass and energy and the resulting damage states compared. This comparison was accomplished by Rutherford backscattering/channeling studies of the damaged crystals.

2. PKA SPECTRA AND CASCADES

Primary knock-on atoms (PKAs) are atoms of the target substance which directly receive energy in a collision with the initial radiation (neutrons, ions, or electrons). The number of PKAs as a function of their energy constitutes the *PKA spectrum*; it is directly determined by the collision kinematics and the differential cross section. For example, the maximum PKA energy is determined by the masses of target and incident particle.

Electron beam irradiation produces only low-energy PKAs because of the great mass difference of electrons from target atoms. Much more energetic PKAs are produced by fast neutrons ($E \geq 1$ MeV), but because the neutrons are uncharged they do not produce very many low-energy PKAs. Although the ion PKA spectrum can be controlled to some extent by selection of ion species and energy, it is clear that one cannot exactly match a realistic neutron PKA spectrum with fast ions since the ions will always produce many more low-energy PKAs than will neutrons.

The dissimilarity of PKA spectra naturally leads to concerns about the suitability of ion beams to simulate neutron damage in materials. At first sight, it appears that for ions a harder PKA spectrum will cause more energy to be deposited in cascades relative to free defects. Careful examination of the subcascade production process reverses this impression.

PKA events have been divided into three categories depending on the recoil energy:

1. low-energy PKAs (below 1 - 2 keV) which produce defect pairs or only small clusters;
2. intermediate-energy PKAs (2 - 12 keV) which produce single cascades; and
3. high-energy PKAs ($E \geq 12$ keV) which produce *multiple* subcascades and free defects.

The boundary energies are not sharply defined, and calculations have been performed to explore the range of uncertainty in the boundary energies.⁽⁷⁾ The probability calculations strongly support the general division into three energy categories; for example, our calculations show that an 18 keV PKA in Si has a probability greater than 90% to launch a subcascade before dropping below ~ 12 keV to form its own subcascade. For this reason, that part of the PKA spectrum which lies above $E_u \sim 12$ keV has no *direct* physical significance or manifestation; PKAs in this range are instead converted into lower-energy subcascades and free defects. This conversion occurs on the fast-collision time-scale ($\sim 10^{-14}$ sec) and is complete before any thermally activated atomic motions. Because of this conversion, the hard neutron spectrum produces free defects and subcascades very much like the damage resulting from ion irradiation.

Because the process discussed here is relatively energetic scattering ($E \gtrsim 12$ keV), it can be modeled with reasonable accuracy by the screened Coulomb potential introduced by Lindhard, Neilsen and Scharff.⁽⁴⁾ Calculations of the probability to launch subcascades and the demonstration that an energy E_u exists such that subcascades are almost certain to be launched for PKA energies above E_u have been described in detail previously.⁽⁷⁾ Similarly, this reference⁽⁷⁾ also discusses the specifics of the sequel calculations which follow the collision sequence in which a PKA having energy greater than E_u is allowed to transfer energy to electrons, low-energy recoils, and subcascade-forming recoils. What will be presented here are the results of such calculations as performed for self-ion bombardment of silicon.

3. EXPERIMENTAL BACKGROUND

3.1 Selection of Target Materials

Single crystal specimens have been selected to permit application of the Rutherford backscattering/channeling technique. The Si specimens were cut from crystals with a $\langle 111 \rangle$ growth axis. Small wafer specimens of approximately 1.5 cm on an edge and 250 μm thick were cleaved along $\{111\}$ directions from larger, 250 μm thick, wafers. Impurity levels in this material are $\sim 10^{15}/\text{cm}^3$.

3.2 Choice of Bombarding Ions and Implant Conditions

Since the experiments utilized ions of different mass, both the energy of the bombarding ions and their flux had to be selected such that the total damage energy deposited into the target and the rate of energy deposition was the same for all ions. In addition, chemical effects from the implanted ions and from point defect concentration gradients induced by proximity of a free surface had to be minimized. Hence, in this study, the inert gas ions ^{20}Ne and ^4He as well as ^1H were employed. The 1 MeV $^{20}\text{Ne}^+$ ions were selected as the reference ion and energy for establishing the damage profile, $S_D(x)$ in the Si crystals. Fluences and energies for the other two species were then determined to provide as close a match as possible to the reference Ne damage profile. There are difficulties with the present range-energy theories but we believe that $S_D(x)$, energy per unit depth deposited into atomic displacements, may be calculated reliably for the region starting at the surface and going into the sample to a depth corresponding to approximately three-quarters of the way to the peak of the displacement damage. Figure 1 shows curves of $S_D(x)$ calculated from a modified EDEP-1 code of Manning and Mueller⁽⁸⁾ for 75 keV ^1H , 0.5 MeV ^4He , and 1 MeV ^{20}Ne , which yield equal energy deposition near the surface of the Si target (0 to 0.3 μm).

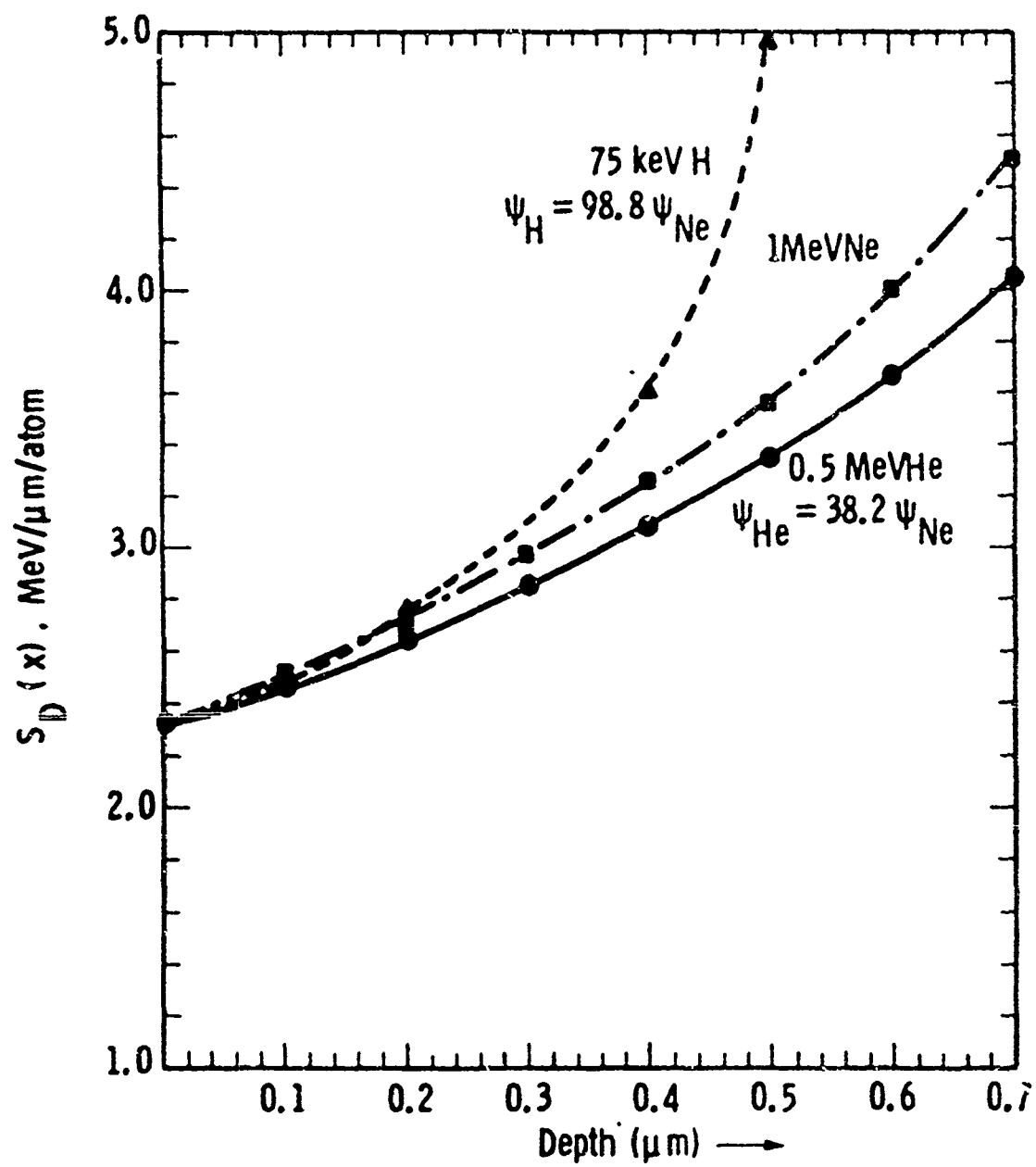


Figure 1. Damage energy deposited per unit length as a function of depth near the surface of a silicon sample for 75 keV ^1H , 0.5 MeV ^4He and 1.0 MeV ^{20}Ne . The appropriate parameters for normalizing to the ^{20}Ne curve are given on the figure.

The $S_D(x)$ curves are normalized at the front surface and the fluences adjusted to agree with ^{20}Ne damage.

Table 1 presents the choice of bombarding ions, energies, and relative fluences selected to produce approximately matching damage profiles over distances of $\sim 0.3 \mu\text{m}$. Also included are the relevant range parameters (R_p and ΔR_p) for each ion, and the maximum transfer energy, T_{max} .

Table 1 - Experimental Parameters

<u>Ion</u>	<u>Energy (MeV)</u>	<u>R_p (μm)</u>	<u>ΔR_p (μm)</u>	<u>ψ/ψ_{Ne}</u>	<u>T_{max} (keV)</u>
^{20}Ne	1.0	1.52	0.168	1	972
^4He	0.5	1.95	0.122	38	219
^1H	0.075	0.71	0.063	99	9.98

4. EXPERIMENTAL PROCEDURES

The final silicon single crystal surfaces utilized for implantation were perpendicular (within 1 to 2°) of the [111] growth direction and were free from mechanical damage. Specimens were implanted 5 to 7° off the [111] axis normal to the surface to minimize channeling effects and, during the bombardment, one-half of each was masked to provide a nonimplanted reference crystal for the channeling studies.

The channeling experiments were performed on a 4.8 meter beam line of the 2 MV Van de Graaff accelerator using 1.5 MeV $^4\text{He}^+$ ions. The ^4He beam was collimated to give a full angular divergence of 0.03°. For the aligned spectra, the He beam was oriented normal to the crystal surface (within 2°) and all spectra were collected at a backscattered angle of 168°. The aligned spectra were obtained in a $\langle 111 \rangle$ axial direction from both the implanted and nonimplanted half of each crystal and the random spectrum was obtained from the nonimplanted half. The random spectrum was measured by setting the symmetry axis 8° from the incoming beam

direction and rotating the sample continuously. Each spectrum was obtained under a constant total He fluence as determined by the backscattered yield from a rotating Au foil, which sampled the beam approximately 7% of the time. The energy scale of the backscattered spectra was converted to a depth scale by employing the electronic stopping powers of ${}^4\text{He}^+$ in Si, with the assumption that the energy loss of the channeled ions is the same as that for ions impinging along a random direction. (9)

5. RESULTS AND DISCUSSION

5.1 Subcascade Spectra

In the calculations, it was considered that a cascade was produced by a recoil of energy greater than $E_{\ell} \sim 0.6 - 2$ keV. As E_{ℓ} is varied through this range, the upper limit E_u (above which multiple cascades are produced) will also vary. However, the general features of the energy partitioning remain constant.

Figure 2 presents the calculated direct and reduced energy spectra for various PKA energies in self-bombarded silicon. The direct spectrum shows the energy deposited in secondary events by PKAs of specified energy. Values of E_{ℓ} and E_u were 1.6 keV and 12 keV, respectively. As the PKA energy rises, a larger fraction of the energy is delivered to energetic ($E > E_u$) secondaries (shaded box). The reduced spectrum is the result of distributing the energy of the shaded box into energy of free defects, cascades, and electrons. A most important finding is that the partitioning of the energy into free defects and cascades, as indicated by the reduced spectra, is almost the same for all recoil energies up to the maximum energy transfer permitted by kinematics. A schematic interpretation of what these results mean in terms of defect and cascade formation is shown in Figure 3. Since the ratio of reduced spectra histogram heights in Figure 2 is almost independent of PKA energy, it is relatively insensitive to the PKA spectrum.

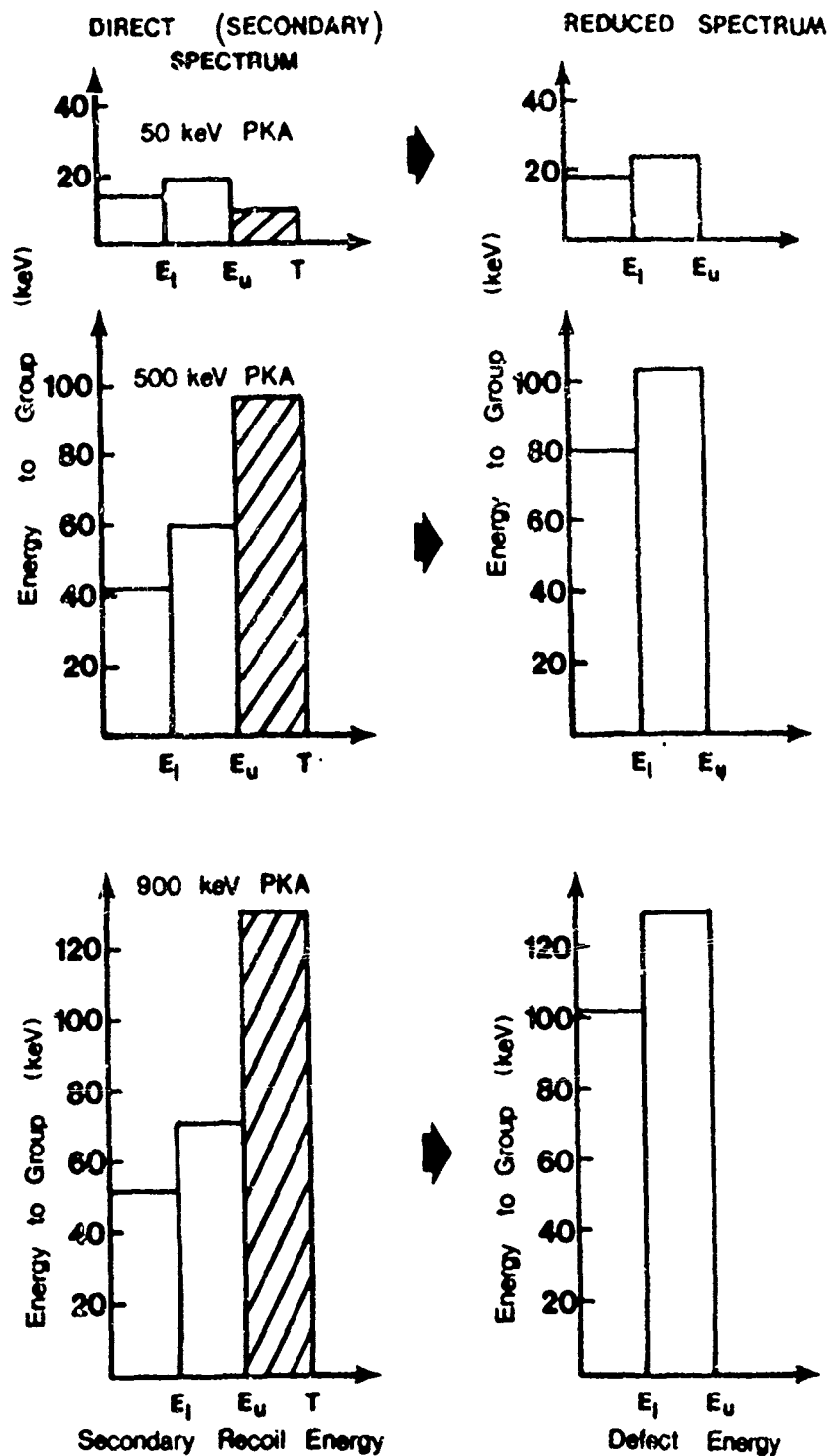


Figure 2. Calculations of the direct and reduced energy spectra for various PKA energies. The direct spectrum shows the energy deposited in secondary events by PKAs of specified energy. E_l is 1.6 keV and E_u is 12 keV in this figure. As the PKA energy rises, a larger fraction of the energy is delivered to energetic ($E > E_u$) secondaries (shaded box). The reduced spectrum results from distributing the energy of the shaded box into energy of free defects, cascades and electrons. In the reduced spectrum, the cascade energy is a constant multiple of the free defect energy, independent of PKA energy.

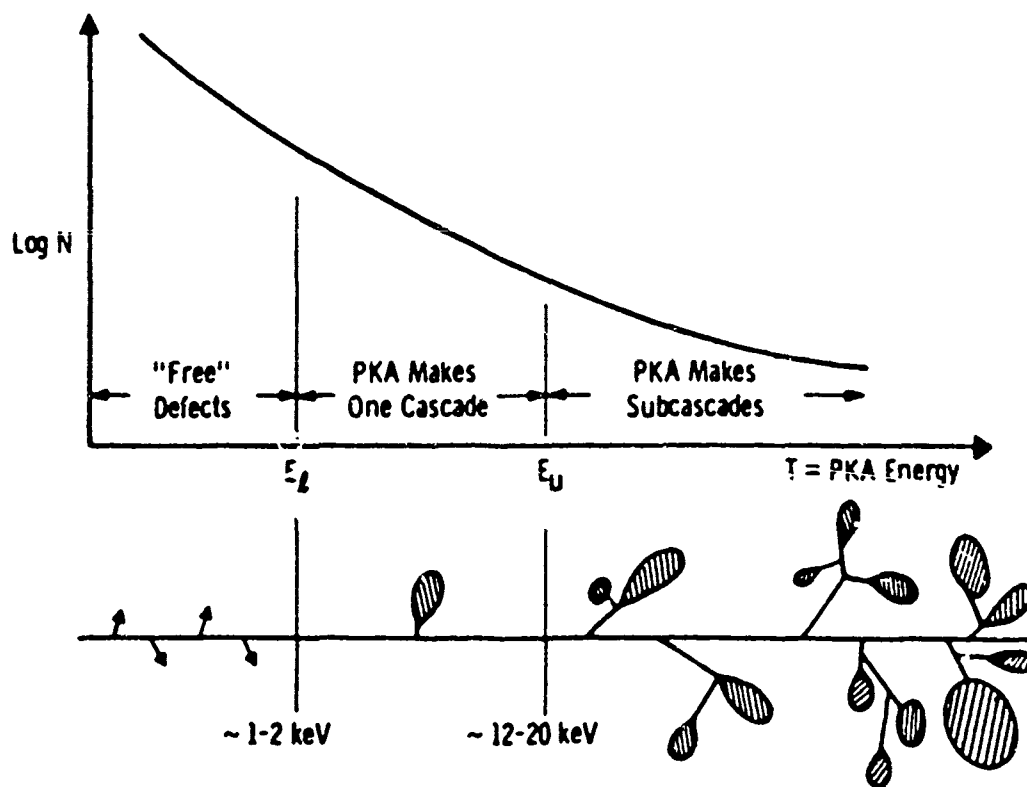


Figure 3. Schematic representation of defect and subcascade formation as a function of PKA energy.

5.2 Backscattering Data

Figures 4 through 6 show aligned backscattered spectra for 1 MeV ^{20}Ne , 0.5 MeV ^4He , and 75 keV ^1H , respectively. Also shown on each figure is a representative aligned spectrum for a nonimplanted (n-i) reference crystal and a random nonaligned spectrum. All yields are normalized with respect to the random spectrum. The peak at zero depth for the aligned spectra is due to the direct backscattering from the surface layer of ions which do not enter a channel and is known as the "surface peak." For the bombarding ions, the surface peak is essentially the same for $1.39 \times 10^{15} \text{ Ne}^+/\text{cm}^2$ and $5.31 \times 10^{16} \text{ He}^+/\text{cm}^2$, but is somewhat larger for $1.37 \times 10^{17} \text{ H}^+/\text{cm}^2$, perhaps due to the increase in fluence. The "errors" in the backscattered spectra are represented by the recorded yield variations on the curves (i.e., the small peaks and valleys).

Comparison of the implanted spectra behind the surface peak reveals very similar behavior up to depths of ~ 400 nm, or slightly beyond the region over which the deposited damage energy was matched (Figure 1). (Note that the large peak at ~ 600 nm in Figure 6 corresponds to the peak of the $S_D(x)$ curve at 640 nm.) The spectra shown in Figures 4 and 6 can be compared more easily at equivalent damage levels by an approach outlined by Merkle et al. ^(10,11) This analysis is frequently applied in channeling experiments and relates the rate of dechanneling to the concentration of defects of type (j) and density (n_j) with a cross section for dechanneling per defect (σ_j). If one normalizes the aligned spectrum by the random spectrum, the normalized yield (χ) represents the dechanneled fraction of ions up to the depth (z), and (1- χ) represents the remaining channeled fraction. Therefore, at any depth z:

$$\frac{d\chi_i}{dz} = (1-\chi_i) \sum_{j=0}^k \sigma_j n_j \quad (1)$$

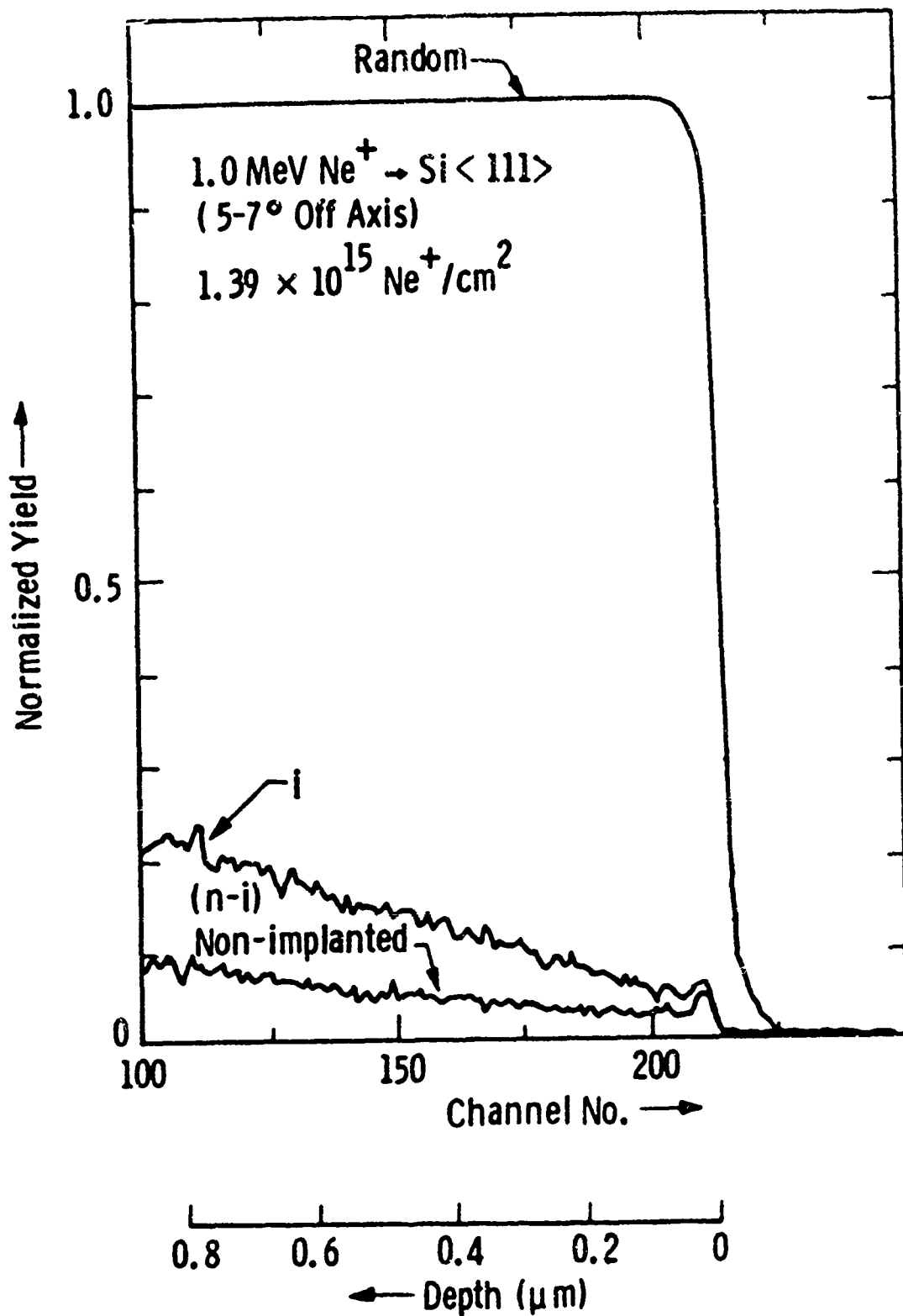


Figure 4. Comparison of normalized yield spectra ($\langle 111 \rangle$ axis) for silicon implanted with 1.0 MeV Ne^+ to a fluence of 1.39×10^{15} ions/ cm^2 and nonimplanted silicon (curve marked (n-i)). Implants were made at approximately 5° off-axis and all spectra were obtained with a 1.5 MeV ^4He beam.

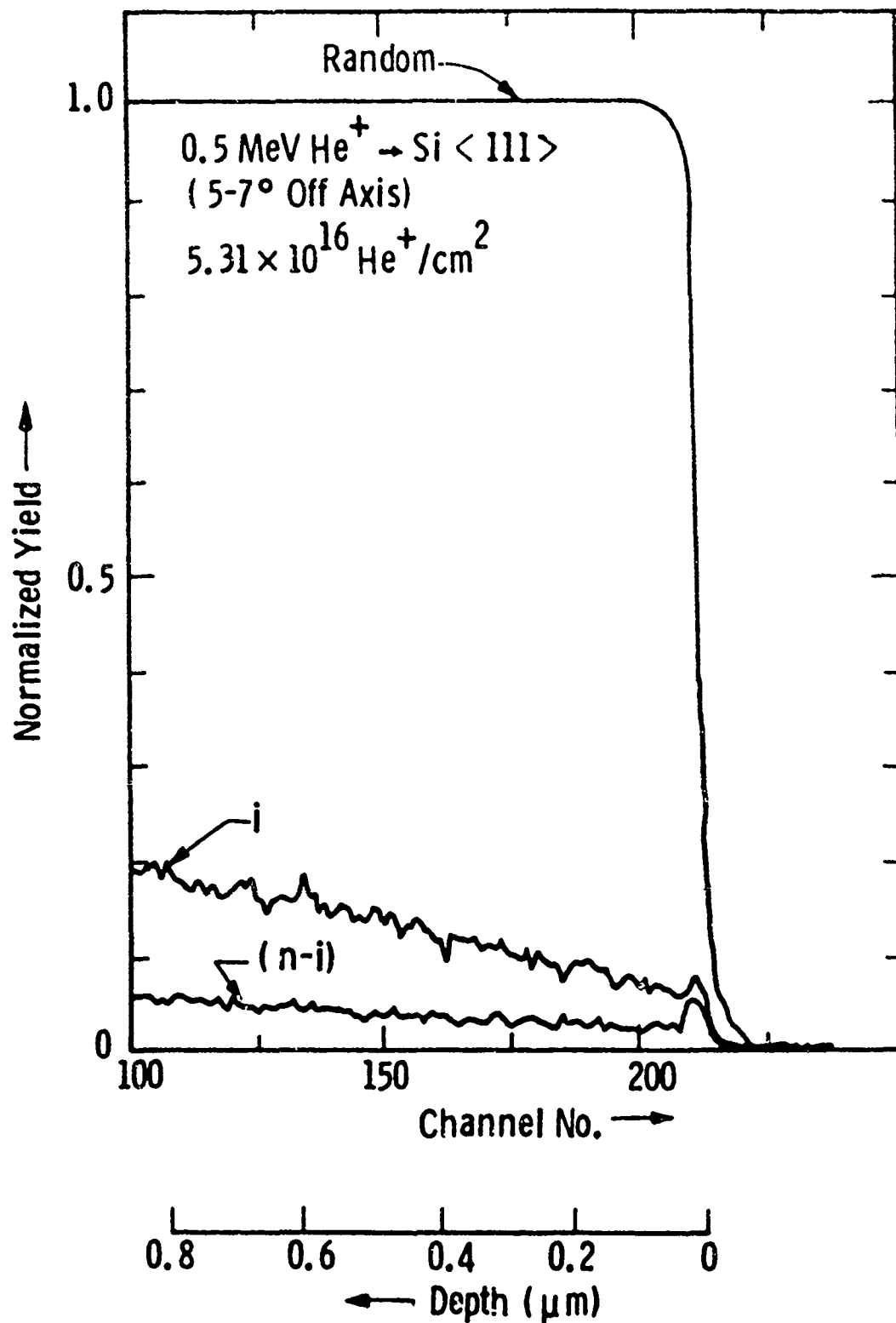


Figure 5. Comparison of normalized yield spectra (<111> axis) for silicon implanted with 0.5 MeV He⁺ to a fluence of 5.31 × 10¹⁶ ions/cm² and nonimplanted silicon (curve marked (n-i)). Implants were made at approximately 5° off-axis and all spectra were obtained with a 1.5 MeV ⁴He beam.

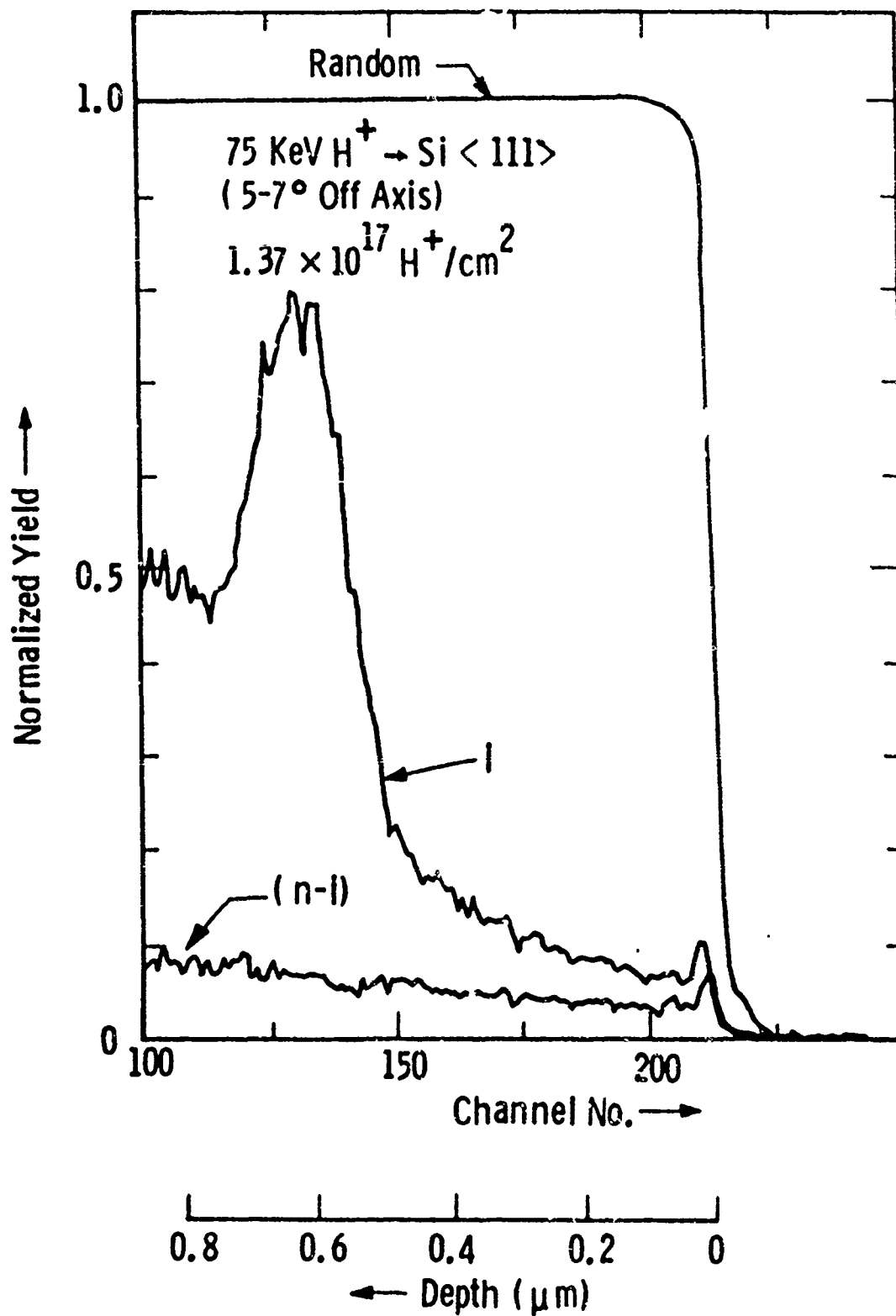


Figure 6. Comparison of normalized yield spectra ($\langle 111 \rangle$ axis) for silicon implanted with 75 keV H^+ to a fluence of 1.37×10^{17} ions/cm² and nonimplanted silicon (curve marked (n-1)). Implants were done at approximately 5° off-axis and all spectra were obtained with a 1.5 MeV 4He beam.

where the subscript (i) refers to the aligned spectrum from the implanted crystal. This equation simply states that the rate of dechanneling at any depth is given by the fraction of ions remaining in the channels times the probability that a single ion will be dechanneled by all the defects of type (j) as it progresses a unit distance along the channel. If the intrinsic dechanneling as measured in the nonimplanted reference crystal is simply additive to that produced by the defects, then equation 1 can be written as

$$\frac{d\chi_i}{(1-\chi_i)} - \frac{d\chi_{n-i}}{(1-\chi_{n-i})} = \left[\begin{array}{c} k \\ \sum_{j=1}^k \sigma_j n_j \end{array} \right] dz \quad (2)$$

where the subscripts (i) and (n-i) refer to the spectra from the implanted and nonimplanted crystals, respectively. This expression strictly holds when the defects introduce dechanneling of the ions into random trajectories without any direct backscattering of ions in the channels. Therefore, according to equation 2, the density of defects and thus the damage level as measured by a channeling experiment is related to the slope of the aligned spectrum.

The quantity $\sum_{j=1}^k \sigma_j n_j$ was calculated using a computer program which first determines $\sum_{j=1}^k$ the slopes of the channeling spectra. The depth range was selected to avoid the proximity of the small surface peak and to extend only to the limit over which the $S_D(x)$ curves were matched.

Figure 7 shows a plot of $\sum_{j=1}^k \sigma_j n_j$ as a function of depth (as determined by equation 2) for the damage level equivalent to 1.39×10^{15} Ne^+/cm^2 . The data are also tabulated in Table 2. It is clear that the extent of dechanneling for the damaged crystals bombarded with 1.0 MeV ^{20}Ne and 0.5 MeV ^4He superimpose, which suggests that equivalent final damage states were produced for these two ions. This further suggests that, provided the deposited damage energy and the rate of energy deposition

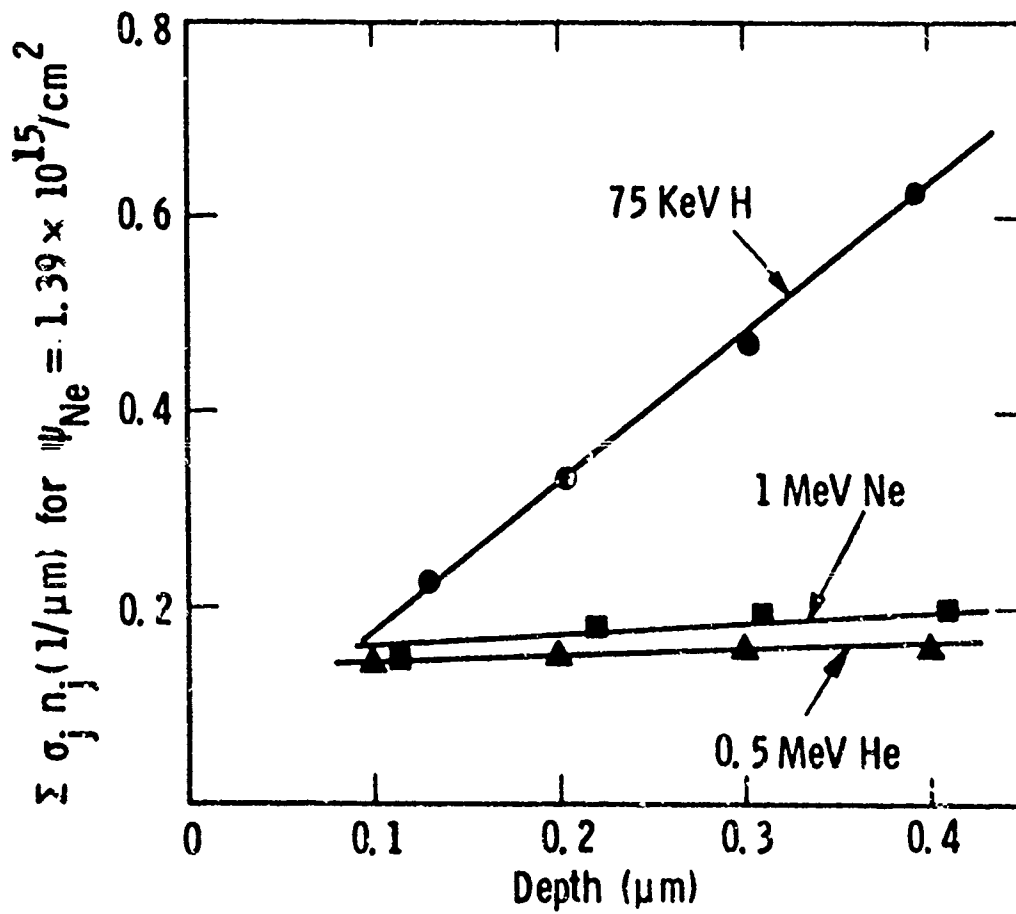


Figure 7. Plot of the dechanneling rate as a function of depth into the crystal for 1 MeV ^{20}Ne , 0.5 MeV ^4He and 75 keV ^1H at the dose equivalent to $1.39 \times 10^{15} \text{ }^{20}\text{Ne}/\text{cm}^2$.

are the same, the damage state produced is essentially independent of the mass and energy of the bombarding ion in the silicon substrate. Such a conclusion is in excellent agreement with data recently reported on ion-bombarded molybdenum. (12)

Table 2 - Dechanneling Rates as a Function of Depth

<u>Implanted Ion</u>	<u>Depth (μm)</u>	<u>$\Sigma \sigma_j n_j$ ($1/\mu\text{m}$)</u>
1.0 MeV ^{20}Ne	0.11	0.14
	0.22	0.18
	0.31	0.19
	0.41	0.19
0.5 MeV ^4He	0.10	0.14
	0.20	0.15
	0.30	0.16
	0.40	0.15
75 keV ^1H	0.13	0.23
	0.20	0.33
	0.30	0.48
	0.39	0.62

The higher slope of the 75 keV ^1H curve corresponding to a greater dechanneling rate, is due to the influence of the large peak observed at 0.6 μm in Figure 6. The implanted hydrogen, with $R_p = 0.71 \mu\text{m}$, is introducing lattice strain which yields an additional contribution to the fraction of dechanneled ions in the near surface region. This does not necessarily indicate that the damage state produced by the 75 keV ^1H as it enters the crystal differs from the states produced by 1.0 MeV ^{20}Ne and 0.5 MeV ^4He . Further work, including electron microscopy, is required to elucidate this question. One might expect that the resultant damage state for ^1H would differ from those produced by ^{20}Ne or ^4He because the recoil spectrum for 75 keV ^1H in silicon would primarily yield free defects. However, since the maximum transfer energy is still ~ 10 keV in silicon, which is considerably larger than E_d , a significant amount of cascade formation could still occur.

An interesting question which is still to be answered concerns the nature of the damage produced by the ion bombardment. It is hoped that transmission electron microscopy (TEM) will be able to determine whether amorphous regions have been produced, or if the dechanneling is primarily due to loop formation, for example. Ligeon⁽¹³⁾ has suggested that 30 keV H implanted into silicon does not produce amorphicity, even at the peak damage region, but that hydrogen bubbles may be contributing to the observed dechanneling. This is difficult to rationalize because of the weak dechanneling effect normally caused by bubbles, and so Ligeon⁽¹³⁾ further suggests that the bubbles are active as generalized stacking faults. TEM characterization of the implanted region may shed light on this question, as it has in previous work on molybdenum.⁽¹²⁾

6. CONCLUSIONS

- Theoretical calculations have shown that, on the fast-collision time scale, the ratio of energy deposited into free defects and subcascades is independent of PKA spectrum and thus of incident ion energy and mass (provided the damage energy deposited and the rate of energy deposition remain the same).

- Channeling experiments on $\langle 111 \rangle$ single crystal silicon implanted with 1.0 MeV $^{20}\text{Ne}^+$, 0.5 MeV $^4\text{He}^+$, and 75 keV $^1\text{H}^+$ ions have shown that equivalent final damage states were produced for all three ions.

- These two results further support the premise that equivalent primary damage states will evolve into statistically equivalent final damage states at high fluences.

7. REFERENCES

1. K. L. Merkle in Radiation Damage in Metals, N. L. Peterson and S. D. Harkness, eds., p. 58, ASM Metals Park, OH (1975).
2. M. T. Robinson and I. M. Torrens, Phys. Rev. B 9 (12), 5008 (1974).
3. J. R. Beeler, Jr., M. F. Beeler and C. V. Parks, Conf. 750989, Proceedings of International Conf. on Radiation Effects and Tritium Technology for Fusion Reactors, p. I-362, Gatlinburg, TN (1976).
4. J. Lindhard, V. Nielsen and M. Scharff, Danske Videnskabskab 36, 10 (1968).
5. J. Lindhard, M. Scharff and H. E. Schiott, *ibid.* 33, 14 (1963).
6. J. Lindhard, V. Nielsen, M. Scharff and P. V. Thomson, *ibid.* 33, 10 (1963).
7. R. M. More and J. A. Spitznagel, "Primary Recoil Spectra and Subcascade Effects in Ion Bombardment Experiments," Radiation Effects, Vol. 60, 27-33 (1982).
8. I. Manning and G. P. Mueller, Computer Physics Communications 7, 85 (1974).
9. J. F. Ziegler, Helium Stopping Powers and Ranges in All Elemental Matter, Vol. IV, Pergamon Press, New York (1977).
10. P. P. Pronko and K. L. Merkle, Applications of Ion Beams to Metals, S. T. Picraux, E. P. Ernisse and F. L. Vook, eds., p. 481, Plenum Press (1974).
11. K. L. Merkle, P. P. Pronko, D. S. Gemmell, R. C. Mikkelsen and J. R. Wrobel, Phys. Rev. B 8 (3), 1002 (1973).

12. J. H. Chang, W. J. Choyke, N. J. Doyle, J. Gregg, P. Hegland, J. N. McGruer, J. A. Spitznagel, J. R. Townsend, and C. F. Tzeng, "Experimental Evidence for Slight Mass Dependence of Final Damage State Due to Energetic Ions," *Radiation Effects* (1982), Vol. 60, pp. 73-84.
13. E. Ligeon and A. Guivarch, *Rad. Effects* 27 (1976).

REPORTS DISTRIBUTION LIST FOR ONR PHYSICS PROGRAM OFFICE
UNCLASSIFIED CONTRACTS

Director Defense Advanced Research Projects Agency Attn: Technical Library 1400 Wilson Blvd. Arlington, Virginia 22209	3 copies
Office of Naval Research Physics Program Office (Code 421) 800 North Quincy Street Arlington, Virginia 22217	3 copies
Office of Naval Research Assistant Chief for Technology (Code 200) 800 North Quincy Street Arlington, Virginia 22217	1 copy
Naval Research Laboratory Department of the Navy Attn: Technical Library Washington, D. C. 20375	3 copies
Office of the Director of Defense Research and Engineering Information Office Library Branch The Pentagon Washington, D. C. 20301	3 copies
U. S. Army Research Office Box 12211 Research Triangle Park North Carolina 27709	2 copies
Defense Documentation Center Cameron Station (TC) Alexandria, Virginia 22314	12 copies
Director, National Bureau of Standards Attn: Technical Library Washington, DC 20234	1 copy
Commanding Officer Office of Naval Research Branch Office 536 South Clark Street Chicago, Illinois 60605	3 copies

Commanding Officer 3 copies
Office of Naval Research Branch Office
1030 East Green Street
Pasadena, California 91101

San Francisco Area Office 3 copies
Office of Naval Research
One Hallidie Plaza
Suite 601
San Francisco, California 94102

Commanding Officer 3 copies
Office of Naval Research Branch Office
666 Summer Street
Boston, Massachusetts 02210

New York Area Office 1 copy
Office of Naval Research
715 Broadway, 5th Floor
New York, New York 10003

Director 1 copy
U. S. Army Engineering Research
and Development Laboratories
Attn: Technical Documents Center
Fort Belvoir, Virginia 22060

ODDR&E Advisory Group on Electron Devices 3 copies
201 Varick Street
New York, New York 10014

Air Force Office of Scientific Research 1 copy
Department of the Air Force
Bolling AFB, D. C. 22209

Air Force Weapons Laboratory 1 copy
Technical Library
Kirtland Air Force Base
Albuquerque, New Mexico 87117

Air Force Avionics Laboratory 1 copy
Air Force Systems Command
Technical Library
Wright-Patterson Air Force Base
Dayton, Ohio 45433

Lawrence Livermore Laboratory 1 copy
Attn: Dr. W. F. Krupke
University of California
P. O. Box 808
Livermore, California 94550

Harry Diamond Laboratories Technical Library 2800 Powder Mill Road Adelphi, Maryland 20783	1 copy
Naval Air Development Center Attn: Technical Library Johnsville Warminster, Pennsylvania 18974	1 copy
Naval Weapons Center Technical Library (Code 753) China Lake, California 93555	1 copy
Naval Training Equipment Center Technical Library Orlando, Florida 32813	1 copy
Naval Underwater Systems Center Technical Library New London, Connecticut 06320	1 copy
Commandant of the Marine Corps Scientific Advisor (Code RD-1) Washington, DC 20380	1 copy
Naval Ordnance Station Technical Library Indian Head, Maryland 20640	1 copy
Naval Postgraduate School Technical Library (Code 0212) Monterey, California 93940	1 copy
Naval Missile Center Technical Library (Code 5632.2) Point Mugu, California 93010	1 copy
Naval Ordnance Station Technical Library Louisville, Kentucky 40214	1 copy
Commanding Officer Naval Ocean Research & Development Activity Technical Library NSTL Station, Mississippi 39529	1 copy
Naval Explosive Ordnance Disposal Facility Technical Library Indian Head, Maryland 20640	1 copy

Naval Ocean Systems Center Technical Library San Diego, California 92152	1 copy
Naval Surface Weapons Center Technical Library Dahlgren, Virginia 22448	1 copy
Naval Surface Weapons Center (White Oak) Technical Library Silver Spring, Maryland 20910	1 copy
Naval Ship Research and Development Center Central Library (Code L42 and L43) Bethesda, Maryland 20084	1 copy
Naval Avionics Facility Technical Library Indianapolis, Indiana 46218	1 copy